



A difunctional interlayer of an activated carbon cloth supported with MoO₂ catalyst for high-rate magnesium–sulfur batteries

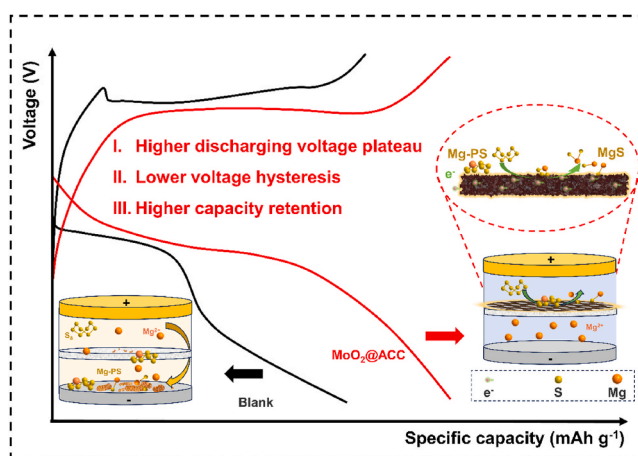
Yaoqi Xu, Fei Wang, Jiayue Wu, Yichao Zhuang, Dongzheng Wu, Jing Zeng^{**}, Jinbao Zhao^{*}

College of Chemistry and Chemical Engineering, Xiamen University, State-Province Joint Engineering Laboratory of Power Source Technology for New Energy Vehicle, State Key Laboratory of Physical Chemistry of Solid Surfaces, Engineering Research Center of Electrochemical Technology, Ministry of Education, Collaborative Innovation Center of Chemistry for Energy Materials, Xiamen, 361005, PR China

HIGHLIGHTS

- The MoO₂@ACC interlayer is prepared by a simple method.
- The shuttle effect of the magnesium-sulfur battery is effectively blocked.
- The kinetics of the magnesium-sulfur battery is significantly improved.
- The magnesium-sulfur battery exhibits a high voltage plateau and high capacity retention of 80.3% at 0.5 C.

GRAPHICAL ABSTRACT



ARTICLE INFO

Keywords:
Mg-S batteries
Interlayer
Adsorb
Catalytic effect
Self-discharge

ABSTRACT

The main challenges faced by magnesium-sulfur (Mg-S) batteries are the polysulfide shuttle effect and slow kinetics of S cathode, causing the severe self-discharge behavior and rapid capacity decay. Herein, we elaborately design a MoO₂-loaded activated carbon cloth (denoted as MoO₂@ACC) functional interlayer to realize high-performance Mg-S batteries. The ACC possesses a remarkable adsorption effect, which can effectively mitigate the polysulfide shuttle effect and enable the Mg-S batteries with a high voltage plateau. Besides, the MoO₂ can observably reduce the polarization during charge/discharge process attributed by the fast reaction kinetics due to the catalytic effect. The Mg-S battery with this MoO₂@ACC interlayer achieves a high energy density and good

^{*} Corresponding author. College of Chemistry and Chemical Engineering, State-Province Joint Engineering Laboratory of Power Source Technology for New Energy Vehicle, State Key Laboratory of Physical Chemistry of Solid Surfaces, Engineering Research Center of Electrochemical Technology, Ministry of Education, Collaborative Innovation Center of Chemistry for Energy Materials, Xiamen University, Xiamen, 361005, PR China.

^{**} Corresponding author. College of Chemistry and Chemical Engineering, State-Province Joint Engineering Laboratory of Power Source Technology for New Energy Vehicle, State Key Laboratory of Physical Chemistry of Solid Surfaces, Engineering Research Center of Electrochemical Technology, Ministry of Education, Collaborative Innovation Center of Chemistry for Energy Materials, Xiamen University, Xiamen, 361005, PR China.

E-mail addresses: zengjing@xmu.edu.cn (J. Zeng), jbzha@xmu.edu.cn (J. Zhao).

<https://doi.org/10.1016/j.jpowsour.2024.234327>

Received 19 January 2024; Received in revised form 27 February 2024; Accepted 7 March 2024

Available online 21 March 2024

0378-7753/© 2024 Elsevier B.V. All rights reserved.

capacity retention (80.3 %) after 100 cycles (0.5 C) and effectively mitigates the Mg–S battery’s self-discharge as well. This work illustrates the significant role of the interlayer with both adsorption and catalytic functions to boost the usability of the Mg–S batteries.

1. Introduction

The revolution in energy technology is driving an increasing demand for advanced energy storage systems [1–3]. Lithium-ion batteries, which have been extensively employed as energy storage devices for portable electronic devices, are unable to satisfy the expectations of an expanding market in the future due to the fact that the resources for cobalt and lithium are running low [4,5]. Therefore, developing alternative batteries based on elements with higher crustal abundance is urgently desired and has become a current research hotspot. Rechargeable magnesium batteries (RMBs) are one type of classical next-generation “beyond Li-ion” battery system among numerous candidates, which are attributed to high abundance of magnesium resources [6–10]. Besides, compared to other alkaline and alkaline earth metals, Mg metal anode has unique advantages of high chemical stability and low tendency to dendritic deposition, which can relieve safety anxiety effectively. Mg metal’s divalent nature enables it to have a high theoretical volumetric capacity ($3833 \text{ mA h cm}^{-3}$), but at the same time, it causes an excessively high charge density for Mg^{2+} ion, resulting in a strong Coulomb interaction between cations and intercalation-type material as well as extremely sluggish Mg^{2+} ion diffusion kinetics, along with the troubles of crystal structure collapse and rapid capacity decay.

As a conversion material, sulfur (S) achieves reversible Mg storage through electrochemical reaction rather than intercalation/deintercalation process, which can inherently avoid sluggish Mg^{2+} ion diffusion behavior in host materials [11–13]. Moreover, when the high crustal abundant S cathodes are matched with Mg anodes, the Mg–S batteries are expected to exhibit a considerable specific energy with low-cost [14]. Following the proposal of the first Mg–S battery by Kim and Muldoon, great efforts have been made in past few years on fundamental reaction mechanism study [15–20]. In general, Mg–S batteries undergo a solid-liquid-solid transformation mechanism during the reaction process, in which the S cathode is first transformed into soluble long-chain magnesium polysulfide (Mg-PS), and then further combines with Mg^{2+} ions to form short-chain Mg-PS, which is ultimately transformed into the final product, MgS [16]. During this process, the severe shuttle effect can not only passivate the Mg anode but also cause irreversible and fast capacity decay [21,22]. Besides, Mg–S batteries face the obstacle of slow diffusion of Mg^{2+} ions in the solid phase during the liquid-solid transition process, leading to the slow kinetic [23,24].

To address the challenges of polysulfide shuttle and sluggish kinetics in Mg–S batteries, designing a highly conductive interlayer with strong adsorption is an effective tactic to mitigate the effect of Mg-PS on the Mg anode and enhance the Mg–S batteries’ electrochemical performance. This is attributed to that the interlayer acts as a physical barrier for Mg-PS to limit the shuttle effect, at the same time, increases the utilization of S and Mg-PS via the conductive effect. According to this design principle, for example, Yu et al. proposed a useful interlayer by depositing an active carbon nanofiber layer on the separator to serve as the upper current collector and a barrier layer for Mg-PS. By capturing and reusing Mg-PS, this interlayer improves the utilization of S and cycling performance of Mg–S batteries [25]. Besides, Dasari Bosubabu et al. introduced a graphene-polyaniline-carbon cloth interlayer into the Mg–S batteries, which has been shown to mitigate the self-discharge observably [26]. Although the current researches have suppressed the shuttle effect and improved the cycling performance of Mg–S batteries, the capacity decay problem is still unsolved and the rate performance remains to be improved [27–29].

In this work, we elaborately design an activated carbon cloth (ACC) supported with MoO_2 catalyst (denoted as “ $\text{MoO}_2@\text{ACC}$ ”) with the

function of adsorption-catalysis. This difunctional interlayer enables Mg–S batteries with both the high capacity retention and good rate performance. This unique interlayer possesses the following advantages: i) $\text{MoO}_2@\text{ACC}$ has a strong adsorption effect on Mg-PS and can effectively block the diffusion of Mg-PS to Mg anode, and effectively reduces the self-discharge behavior. ii) The $\text{MoO}_2@\text{ACC}$ interlayer provides an orderly electron transport network, which can overcome the shortcoming of low conductivity of MoO_2 and improve its electrocatalytic performance. iii) MoO_2 can serve as the catalyst to promote the conversion of Mg-PS, which accelerates the S cathode reaction kinetics, and reduces the polarization during the charge/discharge process and improves capacity retention of Mg–S batteries.

2. Experiment section

2.1. Fabrication of the $\text{MoO}_2@\text{ACC}$

The $\text{MoO}_2@\text{ACC}$ was synthesized by a simple dissolution-drying-carbonization process. Firstly, 9.98 g of $(\text{NH}_4)_2\text{MoO}_4 \cdot 4\text{H}_2\text{O}$ (Sinopharm Chemical Reagent Co., Ltd) was dissolved in 80 mL deionized water to obtain clear solution with a concentration of 0.1 mol/L. The ACC (Guangdong Canrd New Energy Technology Co, Ltd) was divided into round disks of 18 mm and then immersed in the above solution for 1 h via bath sonication. The as-prepared ACC was dried in a vacuum oven at 80°C for 3 h. Finally, the as-prepared ACC was placed in a porcelain boat and heated under an argon atmosphere at 800°C for 4 h with a heating rate of $5^\circ\text{C}/\text{min}$, followed by natural cooling to room temperature to obtain $\text{MoO}_2@\text{ACC}$. The ACC without soaking into the above solution was treated with the same carbonization process to obtain ACC. The details of the interlayer are shown in Table 1.

2.2. Preparation of the cathode

The CMK-3/S material was prepared by the melt diffusion method: 0.6 g of S powder (Sigma-Aldrich) and 0.4 g of CMK-3 (XFNANO) were thoroughly mixed by grinding, then the mixture was encapsulated in a vacuum glass tube and placed in a tube furnace, heated at 160°C for 16 h. The cathode was composed of 80 wt% CMK-3/S, 10 wt% Ketjenblack and 10 wt% polyvinylidene fluoride and was casted on a carbon-coated Al foil. The cathode was further dried at 80°C under vacuum overnight and then was divided into round disks of 12 mm for use. The mass loading of S was $0.8\text{--}1.0 \text{ mg cm}^{-2}$.

2.3. Preparation of the electrolyte and MgS_x

0.5 M Mg [B(hfip) $_4$] $_2$ /DME was chosen as the electrolyte for the Mg–S batteries [30]: The MgS_x were prepared by leaving S powder and Mg powder in the 0.5 M Mg [B(hfip) $_4$] $_2$ /DME electrolyte for 1 week followed by filtration [31].

Table 1
The details of the interlayer.

ACC	Thickness	Mass	The mass loading of MoO_2
	0.199 mm	13 mg–14 mg	$\sim 3 \text{ mg}$ (1.17 mg cm^{-2})

2.4. Preparation of the glass fiber separators and Mg foil electrodes

Glass fiber separators (Whatman, GF/B) were divided round disks of 19 mm and were further dried at 80 °C under vacuum overnight and then was transferred into the glovebox for further use. The pristine Mg foils (200 μm in thickness, >99.9%) were thoroughly polished by 2000 grit sandpapers for three times and then washed with pure DME solvent in an argon-filled Braun glovebox (oxygen and water contents were less than 0.5 ppm). These fresh Mg foils were divided into round disks of 16 mm for use.

2.5. Material characterizations

The surface morphology and elemental distribution of the materials were investigated by scanning electron microscope (SEM, HITACHI TM3030) and energy dispersive X-ray spectrometer (EDS). The crystallographic information was characterized by X-ray diffraction (XRD, Rigaku Corporation, Japan) with a Cu K α radiation. Specific surface area data of the materials were measured by ASAP 2020. Raman tests were performed using a Raman spectroscope (Horiba Xplora) and the excitation intensity is 523 nm. X-ray photoelectron spectroscopy (XPS) spectra were obtained using a PHI Quantum 2000. All Ultra-violet-visible (UV-vis) spectroscopy measurements were used UV-2600 (Japan).

2.6. Electrochemical measurements

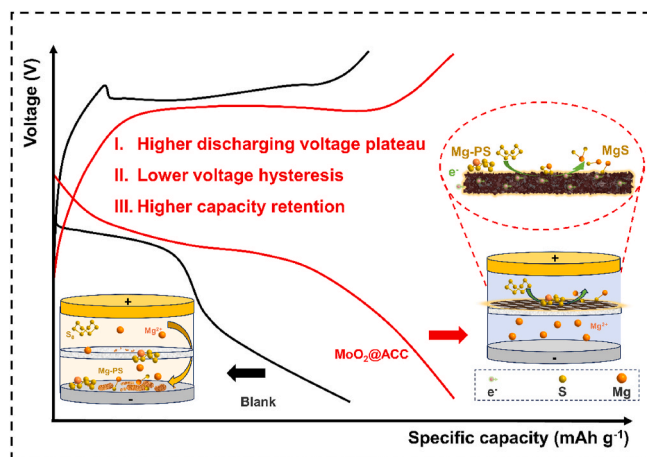
Coin cells of the CR-2016 type were assembled for testing of cycling and rate performances on the Neware standard battery tester. The amount of the electrolyte for coin cells was 120 μL . The MoO₂@ACC interlayer was placed between the S cathode and the separator. The tests of Mg-S full cells were conducted with a charging/discharging voltage range from 0.5 V to 2.55 V. The CV measurements were tested on an electrochemical workstation (CHI 730 E, Chenhua) with a voltage range from 0.5 V to 2.8 V at a scan rate of 0.5 mV s⁻¹. In the galvanostatic intermittent titration technique (GITT) tests, the Mg-S batteries were discharged/charged at 100 mA g⁻¹ for 1 h and paused for 4 h until their voltage decline below than 0.5 V. The temperature for all electrochemical measurements was 25 °C.

2.7. Quantum chemistry calculation methods

Quantum chemistry calculation was performed by Gaussian09 E01 [32]. The functional B3LYP along with D3 Dispersion correction and def 2-SVP basis sets were used to optimize the geometries and obtain the molecular orbital wave function [33–35]. Bond order analysis were performed by Multitwfn [36].

3. Results and discussion

In general, the freshly assembled battery needs to age for a certain time to allow the electrolyte to fully infiltrate the positive and negative materials and thus reduce the interfacial impedance and form a good ion channel. However, Mg-S batteries undergo serious self-discharge during this aging process [31,37]. Active S materials can be dissolved and diffused to the anode, generating Mg-PS through a non-Faraday reaction, causing the passivation of the anode and the depletion of battery capacity (Scheme 1). Therefore, in view of the inhibition of the loss of active material and the diffusion of Mg-PS, we designed a conductive interlayer with excellent adsorption and catalytic effects to enhance Mg-S batteries' electrochemical performance. In detail, the ACC interlayer with good adsorption and conductivity can effectively adsorb dissolved S as well as Mg-PS and reuse them to improve the utilization of cathode materials. Besides, laminated MoO₂ grown on the conductive ACC serves as a catalyst to accelerate the Mg-S battery's reaction kinetics, which is beneficial to reduce polarization and enhance Mg-S



Scheme 1. The classical capacity-voltage curve and internal reaction schematics of Mg-S batteries in blank sample and MoO₂@ACC.

battery cycle stability.

3.1. Study of self-discharge behavior of Mg-S batteries

First, after assembling the Mg-S batteries, we investigate their self-discharge behaviors by aging for 1 h, 3 h, 5 h, and 7 h. Then, the open-circuit voltage (OCV) curves of these Mg-S batteries are recorded by a standard battery tester (Fig. 1a). The OCV of all freshly assembled Mg-S batteries is between 1.70 and 1.73 V, exhibiting their good consistency. Subsequently, the OCV of all the Mg-S batteries drops rapidly to about 1.45 V. The voltage of the Mg-S battery gradually stabilized at about 1.43 V as the resting time increased. The rapid voltage drops during the aging process and the appearance of a stable voltage plateau indicate that Mg-S batteries undergo a severe self-discharge as soon as assembling completion [38]. The Mg-S batteries with different aging times are further charged/discharged at the same rate of 0.2 C (1 C = 1670 mA h g⁻¹) (Fig. 1b and c). After aging for 1 h, 3 h, 5 h and 7 h, the Mg-S batteries can deliver specific capacities of 504 mA h g⁻¹, 389.5 mA h g⁻¹, 317 mA h g⁻¹ and 162.2 mA h g⁻¹, respectively. Interestingly, the capacity of the first discharge plateau around 1.36 V gradually decreases as the aging time increases. The first discharge plateau corresponds to the shift of S₈ to the MgS_x polysulfide (4 ≤ x ≤ 8) during the discharge process, revealing that the active S₈ materials are gradually lost from the positive electrode with the prolongation of the aging time [39]. It is noteworthy that the stabilized self-discharge voltage plateau is similar to the discharge plateau voltage of Mg-S batteries, implying that the reaction occurring during the aging process is the same as the first discharge stage, which means the transformation of S₈ to MgS_x polysulfide (4 ≤ x ≤ 8). In conclusion, excessively long aging process can lead to the loss of the most S material, which ultimately causes the disappearance of the first discharge plateau.

To confirm the conversion of S₈ to Mg-PS during the aging process, we disassemble Mg-S batteries with different aging times and observe the changes of separators (Fig. 1e). As the aging time increases, the color of separators gradually turns yellow, demonstrating the formation of soluble Mg-PS and gradually increases [38]. Furthermore, regarding the Mg-S battery that has a 7-h aging time, yellow solid particles begin to appear on the separator, and this phenomenon can also be found in previous studies [31]. It indicates that during the aging process, the transformation of S₈ to Mg-PS occurs, as well as the further conversion of Mg polysulfide to solid polysulfide. The content of Mg-PS in the separator is further investigated by ex-situ UV-vis (Fig. 1d). The separators with different aging times are immersed in 2 mL DME, and then the clear solution was filtered out and subjected to UV-vis testing. The gradual increase in the absorbance of Mg-PS with the increase in aging times

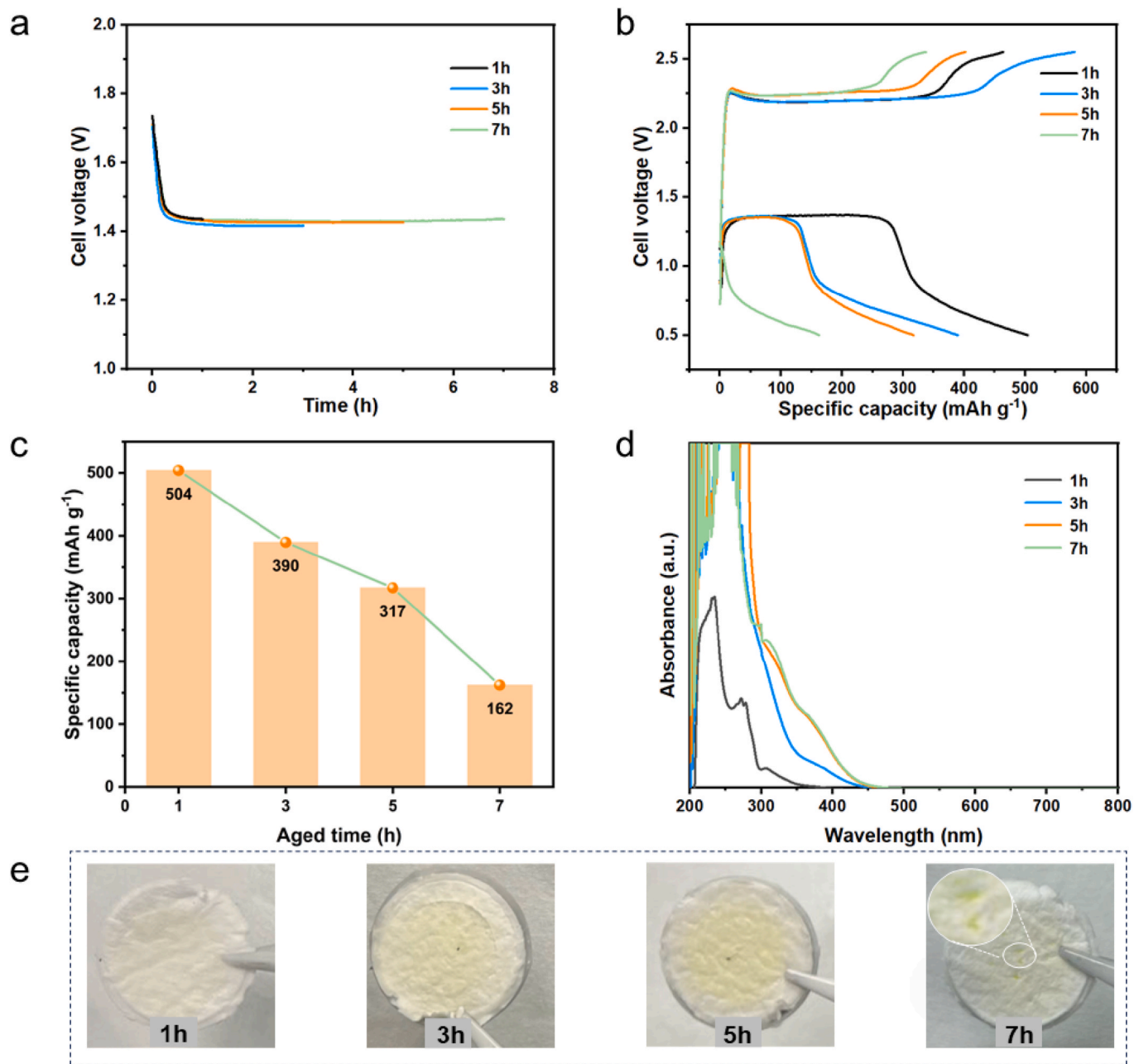


Fig. 1. (a) The OCV test with different aging times. (b) The 1st cycle charge-discharge profiles for Mg-S batteries after different OCV test. (c) 1st cycle discharge capacity for Mg-S batteries after different OCV test. (d) Respective UV-vis spectra in various OCV test. (e) The optical photograph of GF/B in various OCV test.

indicates that the concentration of Mg-PS in the separator rises on account of the ongoing self-discharge. Moreover, the subsequent shuttle effect of soluble Mg-PS also leads to the rapid decay of the capacity of Mg-S batteries (Fig. S1). Therefore, from the perspective of inhibiting the dissolution and diffusion of S and Mg-PS, an interlayer with strong adsorption and catalysis is designed to enhance the kinetics and cycling stability.

3.2. Characterization of the structure and morphology of the interlayer

The preparation process of the MoO₂@ACC interlayer is shown in Fig. 2a. First, the ACC is soaked in 0.1 M ammonium molybdate solution and ultrasonicated for 1 h. After drying, the as-prepared ACC interlayer is heated for 4 h at 800 °C under an Ar atmosphere to obtain the MoO₂@ACC interlayer. As shown in Fig. 2b and c, the ACC exhibits an ordered fiber structure, which provides a continuous electron transport

network [40]. The diameter of a single carbon fiber is about 10 μm, with relatively smooth surface. Furthermore, the BET method is adopted to assess the specific surface area, and the results show that the ACC has a high specific surface area of 922.1 m²/g (Fig. S2 a, b). This unique structure can favorably adsorb and block Mg-PS. The MoO₂@ACC prepared by a simple solution soaking-drying-carbonization method showed a more complex surface morphology (Fig. 2d). The optical photograph (shown in the inset in Fig. 2d) shows that the color of MoO₂@ACC is gold purple, which is clearly different from the original ACC. As shown in Fig. 2d, MoO₂ presents a sheet-like structure uniformly loaded on the surface of the ACC, which provides more voids for MoO₂@ACC. The unique structure is favorable for electrolyte infiltration and ion transport and is more effective in blocking Mg-PS [41]. In addition, the uniformly distributed MoO₂ on the ACC substrate are more likely to obtain electrons to form more active sites with electrocatalytic functions. Besides, EDS analysis

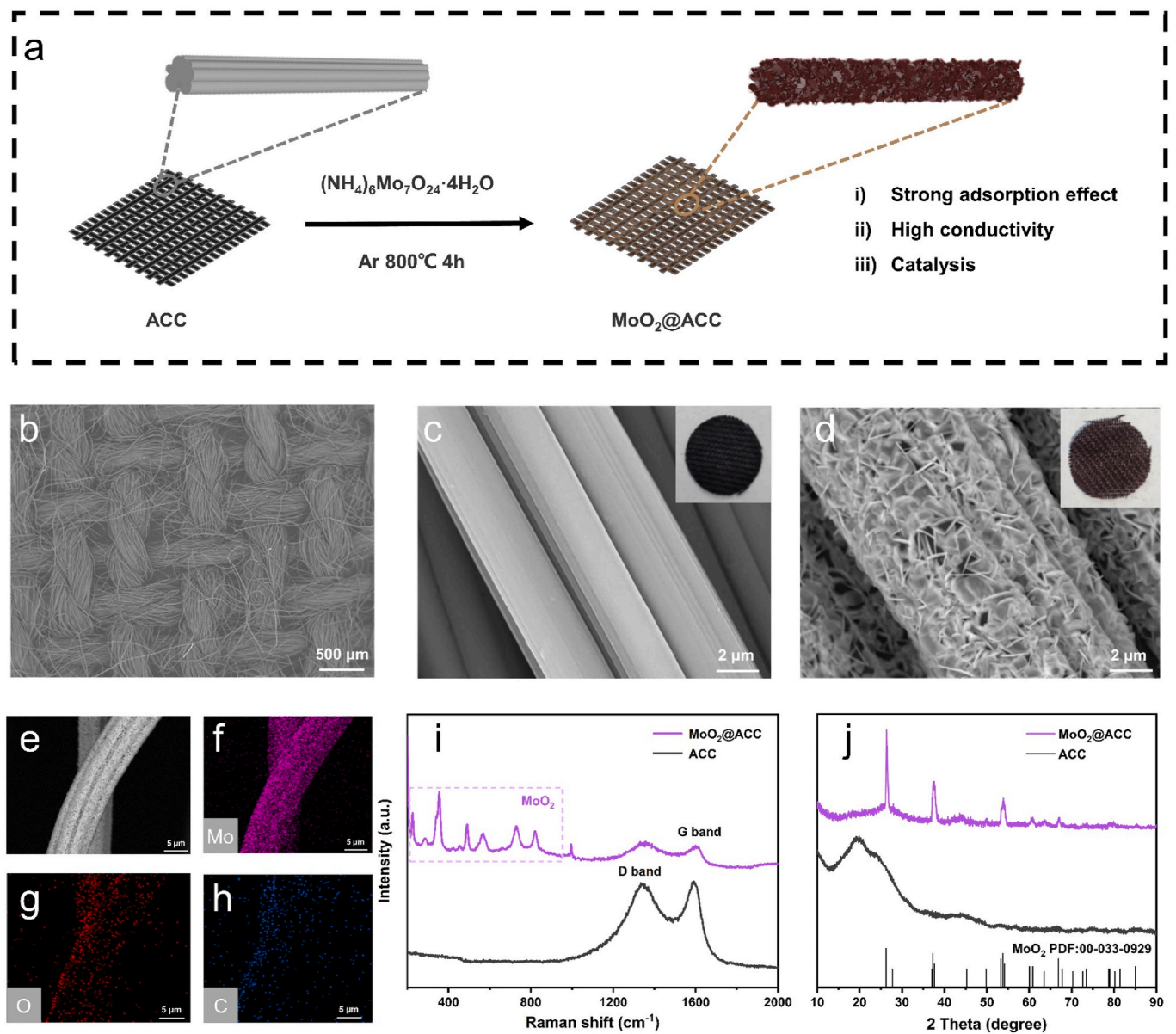


Fig. 2. a) Schematic illustration of the preparation procedure of MoO₂@ACC. SEM images of b, c) ACC and d) MoO₂@ACC. The inset of c, d) is the optical photograph of ACC and MoO₂@ACC. e-h) EDS mapping of elements molybdenum, oxygen, carbon of the MoO₂@ACC fiber. i) XRD patterns of ACC and MoO₂@ACC. j) Raman spectra of ACC and MoO₂@ACC.

(Fig. 2e–h) also indicates the uniform distribution of Mo, O and C elements on the MoO₂@ACC. The structure of MoO₂@ACC was investigated by Raman spectrum and XRD. As shown in Fig. 2i, the two typical peaks of 1600 cm⁻¹ and 1356 cm⁻¹ can be attributed to the G-band of graphitized carbon and the D band of disordered carbon, respectively [42,43]. Besides, a clear Raman signal of MoO₂ is exhibited in the range of 200–800 cm⁻¹ [42]. The XRD pattern (Fig. 2j) shows the characteristic peaks of MoO₂ (≈26.4, 37.4, 54, 60.45 and 67.0°), which matches with the standard card of the MoO₂ crystal phase (PDF#00-033-0929). All of these results, in conclusion, further demonstrate the successful synthesis of MoO₂@ACC.

3.3. Verification of adsorption function

As shown in Fig. 3a, the adsorption effect of ACC and MoO₂@ACC interlayers on Mg-PS is investigated. Mg-PS is synthesized according to the literature, and the original color of the Mg-PS solution is clearly yellow [31]. Subsequently, the ACC and MoO₂@ACC interlayers are

immersed into the Mg-PS solution, respectively. After aging for 24 h, the colors of the two solutions are both obviously lighten, while the discoloration of solution with MoO₂@ACC interlayer is more obvious. The solutions after static adsorption were detected by UV–vis absorption spectroscopy (Fig. 3a). The original Mg-PS solution exhibits a strong absorbance of S₈²⁻ (260–280 nm), S₆²⁻ (~355 nm), and S₄²⁻ (~410 nm) ions [27,44,45]. The MoO₂@ACC interlayer has a stronger adsorption effect compared to ACC, and the peak of Mg-PS is observably weakened. Moreover, the intensity of S₆²⁻ and S₄²⁻ almost disappeared, indicating that MoO₂@ACC is an effective blocking layer for Mg-PS adsorption. To further verify the interaction between Mg-PS and MoO₂@ACC, the MoO₂@ACC interlayer is first immersed in Mg-PS solution for 3 days and then characterized by XPS. As shown in Fig. 3b, MoO₂@ACC before soaking shows characteristic Mo 3d peaks and the four typical peaks that can be attributed to Mo⁴⁺ (229.50 eV and 232.76 eV) and Mo⁶⁺ (231.60 eV and 234.80 eV). The Mo⁶⁺ could be generated from the oxidation of MoO₂ [46–48]. The MoO₂@ACC immersed in Mg-PS shows that both binding energy is slight shift and relative intensity is changed,

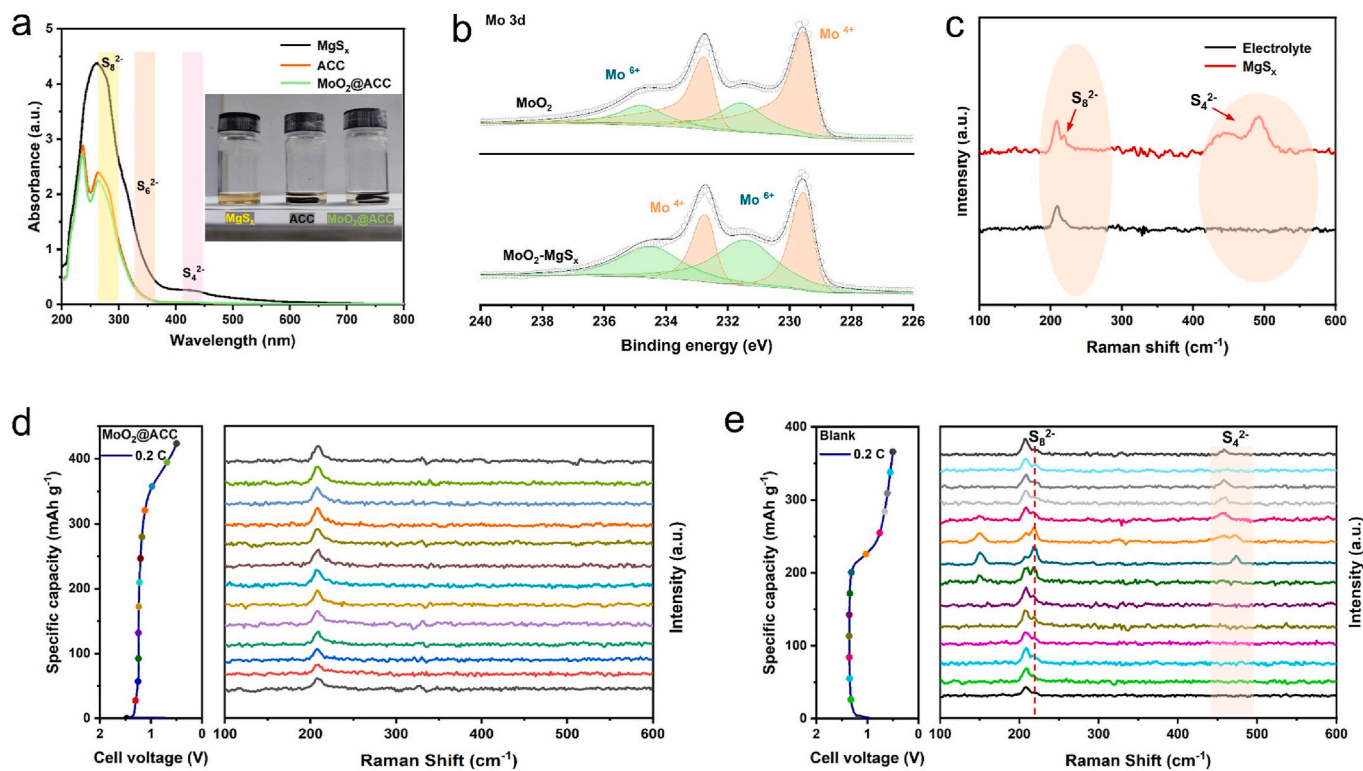


Fig. 3. a) UV-vis spectra and visual adsorption (inset) of the MgS_x solutions before and after exposure to ACC and $\text{MoO}_2@/\text{ACC}$ for 2 h. b) XPS spectra of Mo 3d of $\text{MoO}_2@/\text{ACC}$ before and after immersion. c) Raman analyses of pure electrolyte and the electrolytes with MgS_x . In-situ Raman spectra of the Mg-S cell at 0.2 C d) with $\text{MoO}_2@/\text{ACC}$ and e) without $\text{MoO}_2@/\text{ACC}$.

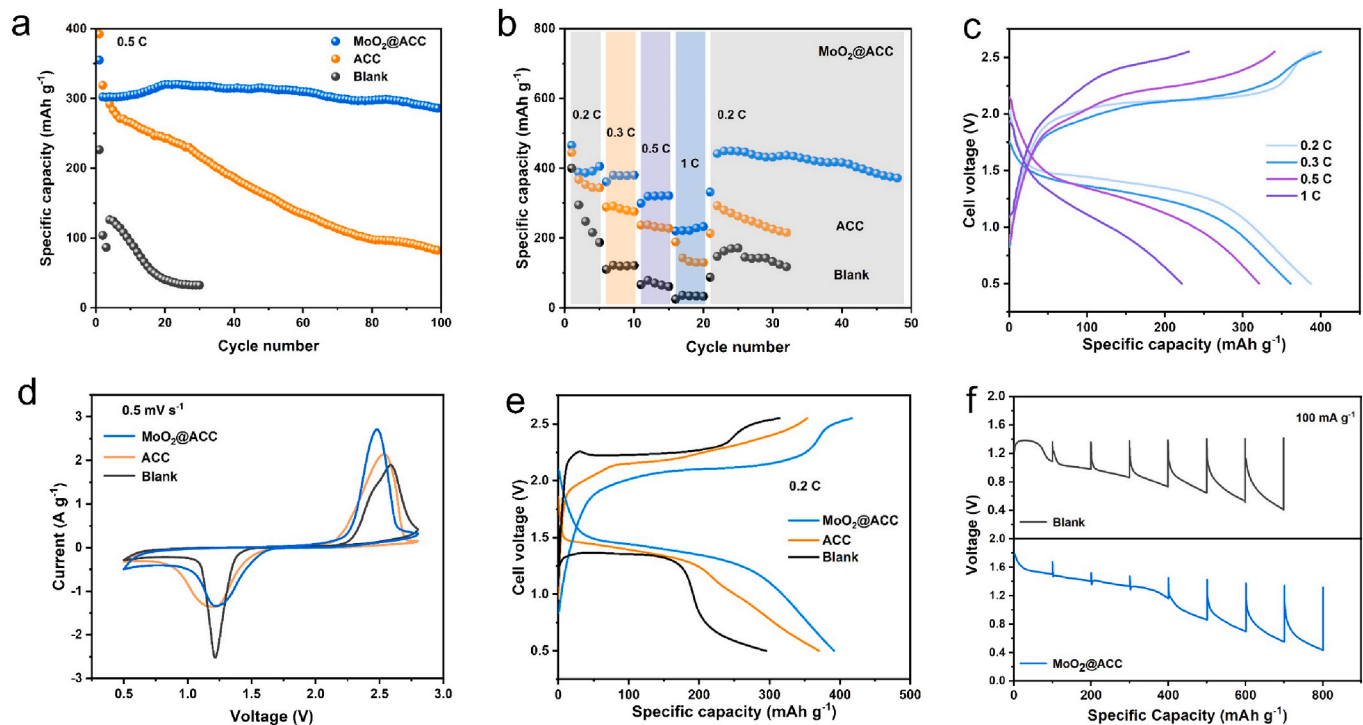


Fig. 4. a) Comparison of cycling performance of the Mg-S batteries equipped with different interlayer. b) Rate performance of the Mg-S batteries with $\text{MoO}_2@/\text{ACC}$, ACC and blank at a current density at 0.2 C, 0.3 C, 0.5 C, 1 C, and 0.2 C. c) Charge/discharge profiles of the $\text{MoO}_2@/\text{ACC}$ cell at different rates. d) CV scans of the three types of Mg-S batteries at a scan rate of 0.5 mV s⁻¹. e) Charge/discharge profiles of the three types of Mg-S batteries at a current density of 0.2 C. f) GITT curves of the Mg-S batteries without $\text{MoO}_2@/\text{ACC}$ and with $\text{MoO}_2@/\text{ACC}$.

in which the peak of Mo^{6+} is slight shifted toward the direction of lower binding energy and its intensity is enhanced, while the peak intensity of Mo^{4+} is weakened, implying that the $\text{MoO}_2@\text{ACC}$ can interaction with Mg-PS and anchoring the Mg-PS [28].

In addition, Mg-PS species identification via Raman spectroscopy was done. First, the electrolyte with Mg-PS is detected by Raman (Fig. S3) and the characteristic peaks of the Mg-PS are marked out. As shown in Fig. 3c, Raman spectra in the electrolyte with Mg-PS and pure electrolyte are compared, and the typical species in Mg-PS have been assigned. Raman spectra indicates that the peak of MgS_8 appears around 221 cm^{-1} and the broad peak at $450\text{--}490\text{ cm}^{-1}$ is ascribed to MgS_4 [18, 49]. Subsequently, the blocking effect of the $\text{MoO}_2@\text{ACC}$ interlayer is further investigated by focusing on the changes of the separator at the anode side during the discharge process via the in-situ Raman spectra technique (Fig. 3d and e). There is no obvious characteristic peak of Mg-PS in the anode electrode of $\text{MoO}_2@\text{ACC}$ interlayer Mg-S battery during the discharging at 0.2 C, disclosing that $\text{MoO}_2@\text{ACC}$ restricts soluble Mg-PS diffusion to the Mg anode. As Mg-S batteries are used without $\text{MoO}_2@\text{ACC}$, the MgS_8 peak remains, indicating a serious shuttle effect. At the same time, the concentration of Mg-PS initially rose and then fell as the discharge continued. To sum up, $\text{MoO}_2@\text{ACC}$ has excellent adsorption properties for Mg-PS, inhibiting the migration of dissolved Mg-PS to the Mg metal anode.

3.4. Electrochemical performance

0.5 M Mg [B(hfip) $_4$] $_2$ /DME is used as the electrolyte in the electrochemical test [30], and the performance of the electrolyte is examined by Mg symmetric cells (Fig. S4). The morphology and elemental distribution of cathode CMK-3/S are shown in Fig. S5. As shown in Fig. 4a, at a high rate of 0.5 C, the Mg-S battery with $\text{MoO}_2@\text{ACC}$ interlayer delivers a specific capacity of 355.1 mA h g^{-1} in the first cycle and possesses the best capacity retention of 80.3% after 100 cycles with a remarkable remaining capacity of 286.3 mA h g^{-1} . Nevertheless, the Mg-S battery with ACC interlayer possesses a poorer capacity retention of 21.2% and the discharge capacity of 78 mA h g^{-1} after 100 cycles. In sharp contrast, the Mg-S battery without modification exhibits a specific capacity of about 30 mA h g^{-1} only after 30 cycles, indicating the irreversible and rapid capacity decay for unmodified Mg-S batteries. Besides, Fig. S8 displays the corresponding contribution capacity contributions of the ACC and $\text{MoO}_2@\text{ACC}$ interlayer without cathode at the same current density of 0.5 C. It can be seen that the stable capacity of $\text{MoO}_2@\text{ACC}$ and ACC is less than 10 mA h g^{-1} , indicating that the capacity contribution of the interlayer can be ignored. Fig. S7a shows the charging/discharging curves of the Mg-S battery with the $\text{MoO}_2@\text{ACC}$ interlayer for the first 5 cycles. The high consistency of the discharging curves from the second to the fifth cycle suggests the great reversibility of the Mg-S battery with the $\text{MoO}_2@\text{ACC}$ interlayer. Besides, the voltage gap between charge curve and discharge curve gradually decreases, exhibiting the activation process of MoO_2 catalysis during charge/discharge [13]. Compared with Figure S7b, Figure S7a shows that the presence of MoO_2 can indeed reduce the polarization of the Mg-S batteries during cycling compared to the ACC group, demonstrating the catalytic effect of MoO_2 [50,51]. Notably, the capacity contribution of the blank group during the discharge process is mainly contributed by the higher voltage plateau (1 V) and the ramp region ($<1\text{ V}$) (Fig. S7c). With the battery cycle progresses, the capacity of the higher voltage plateau of the Mg-S cell in the blank group decays severely and finally even disappears. In contrast, the capacity of this higher voltage plateau in the Mg-S batteries with the $\text{MoO}_2@\text{ACC}$ interlayer hardly decays, which can make full use of the high energy density of Mg-S batteries [52].

Mg-S batteries face shuttle effect and polarization problems of Mg-PS, which leads to rapid loss of active material during cycling, resulting in rapid capacity degradation [53,54]. Even with the introduction of conductive ACC, the capacity retention of Mg-S batteries is still very

low. Surprisingly, the MoO_2 catalyst has the potential to significantly speed up the conversion of Mg-PS, which further greatly improves the capacity retention of Mg-S batteries. Furthermore, as shown in Fig. 4b and c, the Mg-S battery exhibits discharge capacities of 387.3 mA h g^{-1} , 361.4 mA h g^{-1} , 321.1 mA h g^{-1} and 221.7 mA h g^{-1} at the rate of 0.2 C, 0.3 C, 0.5 C and 1 C, respectively. When the rate reverts to 0.2 C, the Mg-S batteries still exhibit an outstanding capacity retention, demonstrating the excellent rate performance and kinetics of Mg-S battery with the $\text{MoO}_2@\text{ACC}$ interlayer. More kinetics information on the conversion of Mg-PS is comparatively investigated by cyclic voltammetry (CV) (Fig. 4d). The Mg-S battery with $\text{MoO}_2@\text{ACC}$ interlayer shows the highest peak oxidation current and the lowest peak oxidation potential compared to others at a scan rate of 0.5 mV s^{-1} , verifying a remarkable improvement of $\text{MoO}_2@\text{ACC}$ interlayer in kinetic behavior and active material utilization. Moreover, Fig. 4e indicates that the Mg-S battery exhibits the lowest charge/discharge polarization and the highest specific capacity of 391 mA h g^{-1} at the rate of 0.2 C, which are in perfect agreement with the CV test results as expected. The discharge kinetics behavior of Mg-S battery with $\text{MoO}_2@\text{ACC}$ interlayer is investigated by constant current intermittent titration. As shown in Fig. 4f, the Mg-S battery with $\text{MoO}_2@\text{ACC}$ shows an observably lower polarization and higher specific discharge capacity than that of the blank, indicating that $\text{MoO}_2@\text{ACC}$ interlayer can not only accelerate the diffusion of Mg^{2+} ions and enhance the dynamics of Mg-S batteries, but also improve the utilization of active materials. In addition, we also added relevant calculations to demonstrate the catalytic effect of MoO_2 on S_8 and MgS_8 , as shown in Fig. S10. The calculated results show that S_8 and MgS_8 tend to interact with Mo atoms in MoO_2 , leading to a change in the electronic structure of S_8 and MgS_8 , which in turn leads to the breakage of S-S bonds in S_8 and MgS_8 . The results show that MoO_2 has both adsorption and catalytic effects, which is consistent with the electrochemical experiments. In brief, $\text{MoO}_2@\text{ACC}$ interlayer has a strong adsorption effect on Mg-PS and catalyzes the conversion of Mg-PS, which is benefit to the Mg-S batteries in the reduction of polarization, and the enhancement of capacity retention, as well as the improvement of rate performance.

3.5. Self-discharge tests

As was previously established, as magnesium sulfur batteries age, they experience tremendous self-discharge. (Fig. 5a). To verify the blocking effect of the $\text{MoO}_2@\text{ACC}$ interlayer on the self-discharge of Mg-S batteries, the assembled Mg-S batteries are aged for 100 h, and the voltage changes of the batteries are monitored during the aging process. The Mg-S battery with $\text{MoO}_2@\text{ACC}$ interlayer shows an OCV of $\sim 2.05\text{ V}$, which is much higher than that of the blank of 1.71 V (Fig. 5 b). The voltage of the blank drops rapidly at first, and then gradually stabilizes at about 1.39 V , which is due to the rapid dissolution of the S cathode and Mg-PS, resulting in a severe self-discharge behavior [37,55]. In sharp contrast, the Mg-S battery with $\text{MoO}_2@\text{ACC}$ interlayer shows a slow voltage drop during the aging stage, indicating that the S and Mg-PS losses are significantly suppressed, and the self-discharge is significantly weakened. After aging for 100 h, the Mg-S batteries undergo a discharge test at a rate of 0.1 C. The Mg-S battery with $\text{MoO}_2@\text{ACC}$ interlayer exhibits a complete Mg-S battery discharge curve, whereas the discharge curve of the blank sample has only one slop. According to the mechanism of Mg-S batteries, the first slope corresponds to the transition from S to soluble long-chain Mg-PS, the plateau region corresponds to the transition from soluble long-chain Mg-PS to short-chain Mg-PS, and the last slope corresponds to the transition from short-chain Mg-PS to MgS [55–58]. The S cathode of the unmodified Mg-S battery is almost depleted after aging for 100 h, and the soluble Mg-PS continue to diffuse and deplete. When the battery is discharged, only a few short-chain Mg-PS are transformed to the final product MgS , and the capacity loss was severe. On the contrary, the $\text{MoO}_2@\text{ACC}$ interlayer can adsorb and block the dissolved S and Mg-PS at the cathode side to avoid their further diffusion to the Mg metal

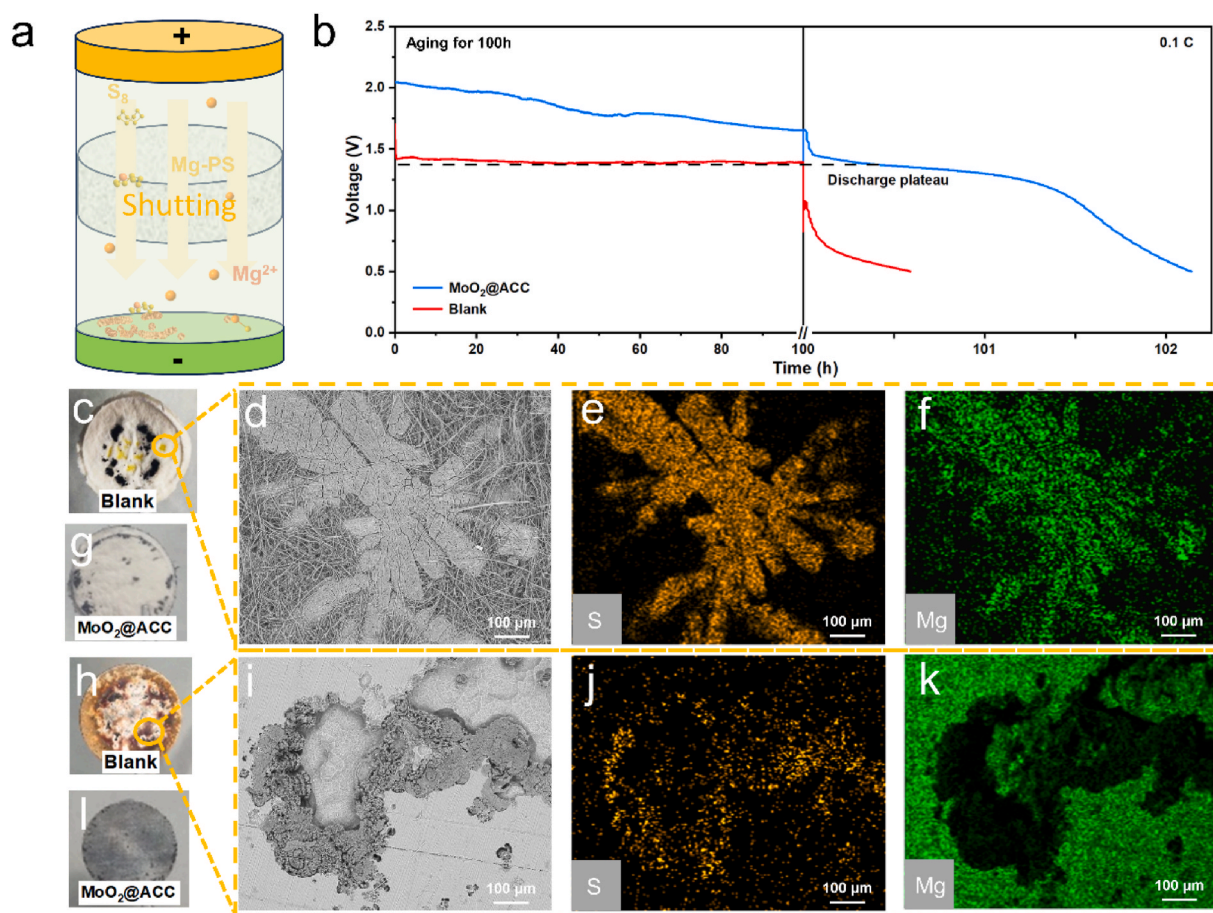


Fig. 5. a) Schematic illustration of the self-discharge in Mg–S batteries. b) Comparison of voltage curves of Mg–S batteries with and without the MoO₂@ACC interlayer (aging for 100 h and discharging at 0.1 C). c) The ex-situ optical image of the GF separator in the blank Mg–S battery. d) The SEM image and e, f) the EDS mapping images of the GF separator in the blank Mg–S battery. g) The ex-situ optical image of the GF separator in the Mg–S battery with the MoO₂@ACC interlayer. h) The ex-situ optical image of the Mg foil in the blank Mg–S battery. i) The SEM image and j, k) the EDS mapping images of the Mg foil in the blank Mg–S battery. l) The ex-situ optical image of the Mg foil in the Mg–S battery with the MoO₂@ACC interlayer.

anode, preventing the self-discharge of Mg–S batteries effectively. A complete discharge process for Mg–S battery with MoO₂@ACC interlayer can still occur after a long aging period, and the discharge capacity is three times higher than that of the unmodified Mg–S battery.

These two discharged completely Mg–S batteries were further disassembled immediately to observe the practical influence of shuttle effect on the separators and Mg anodes (Fig. 5c–k). The separator of the unmodified Mg–S battery shows distinct yellow granular precipitates. EDS analysis suggest that the yellow granular precipitation shows a high content of Mg and S elements, indicating that numbers of solid Mg-PS is deposited on the separator, causing irreversible capacity loss. As for the Mg anode of the unmodified Mg–S battery, the optical image also shows a large yellow area, which is presumed to be the reaction products between Mg-PS and Mg anode. Besides, the EDS analysis show the presence of large amounts of S as well. In contrast, the Mg–S battery with MoO₂@ACC interlayer shows no apparent change in either the separator or the Mg anode (Fig. S9). It shows that the Mg–S battery with MoO₂@ACC interlayer can resist prolonged aging time and keep S and Mg-PS away from the anode.

4. Conclusions

In this work, a difunctional MoO₂@ACC interlayer with adsorption-catalysis effect has been designed to achieve a remarkable capacity retention in Mg–S batteries, maintaining a specific capacity of 286.3 mA h g⁻¹ for 100 cycles at a high rate of 0.5 C. The MoO₂@ACC interlayer

has a strong adsorption of Mg-PS, which can effectively inhibit the shuttle effect of S cathode and the self-discharge of Mg–S batteries. Moreover, the MoO₂@ACC interlayer can not only accelerate the reaction kinetics in Mg–S batteries, but also catalyze the conversion of Mg-PS, along with reducing the charging/discharging polarization of Mg–S batteries. This work overcomes the defect of low conductivity of metal oxides by using highly conductive activated carbon cloth, and provides a promising way to achieve high performance Mg–S batteries through bifunctional interlayer modification.

CRediT authorship contribution statement

Yaoqi Xu: Writing – original draft, Formal analysis, Data curation, Conceptualization. **Fei Wang:** Writing – review & editing, Data curation. **Jiayue Wu:** Writing – review & editing, Data curation. **Yichao Zhuang:** Writing – review & editing, Data curation. **Dongzheng Wu:** Writing – review & editing, Data curation. **Jing Zeng:** Writing – review & editing, Software, Resources, Project administration, Funding acquisition. **Jinbao Zhao:** Writing – review & editing, Supervision, Software, Resources, Project administration.

Declaration of competing interest

The authors declare that they have no known competing financial interests or personal relationships that could have appeared to influence the work reported in this paper.

Data availability

The authors do not have permission to share data.

Acknowledgments

The authors gratefully acknowledge the National Key Research and Development Program of China (No. 2021YFB2400300), Natural Science Foundation of China (Nos. 21875198, 22005257, and 22021001), Natural Science Foundation of Fujian Province of China (No.2020J05009) for financial support. We are grateful to Dr. Yuhao Hong at Tan Kah Kee Innovation Laboratory (IKKEM), Center for Micro-nano Fabrication and Advanced Characterization, Xiamen University for help with the XPS measurement.

Appendix A. Supplementary data

Supplementary data to this article can be found online at <https://doi.org/10.1016/j.jpowsour.2024.234327>.

References

- X. Zhang, Y.A. Yang, Z. Zhou, Towards practical lithium-metal anodes, *Chem. Soc. Rev.* 49 (2020) 3040–3071, <https://doi.org/10.1039/c9cs00838a>.
- J.B. Goodenough, Y. Kim, Challenges for rechargeable Li batteries, *Chem. Mater.* 22 (2010) 587–603, <https://doi.org/10.1021/cm901452z>.
- Z. Zhao-Karger, M.E.G. Bardaji, O. Fuhr, M. Fichtner, A new class of non-corrosive, highly efficient electrolytes for rechargeable magnesium batteries, *J. Mater. Chem. A* 5 (2017) 10815–10820, <https://doi.org/10.1039/c7ta02237a>.
- K. Turcheniuk, D. Bondarev, V. Singhal, G. Yushin, Ten years left to redesign lithium-ion batteries Reserves of rare metals used in electric-vehicle cells are dwindling, so boost research on iron and silicon alternatives, urge Kostiantyn Turcheniuk and colleagues, *Nature* 559 (2018) 467–470, <https://doi.org/10.1038/d41586-018-05752-3>.
- J.M. Tarascon, M. Armand, Issues and challenges facing rechargeable lithium batteries, *Nature* 414 (2001) 359–367, <https://doi.org/10.1038/35104644>.
- H.D. Yoo, I. Shterenberg, Y. Gofer, G. Gershinshy, N. Pour, D. Aurbach, Mg rechargeable batteries: an on-going challenge, *Energy Environ. Sci.* 6 (2013) 2265–2279, <https://doi.org/10.1039/c3ee40871j>.
- F. Wang, H.M. Hua, D.Z. Wu, J.L. Li, Y.Q. Xu, X.Z. Nie, Y.C. Zhuang, J. Zeng, J. B. Zhao, Solvent molecule design enables excellent charge transfer kinetics for a magnesium metal anode, *ACS Energy Lett.* (2022) 780–789, <https://doi.org/10.1021/acsenergylett.2c02525>.
- J. Zeng, J.B. Zhao, Y.C. Zhuang, D.Z. Wu, F. Wang, Y.Q. Xu, Tailoring a hybrid functional layer for Mg metal anodes in conventional electrolytes with a low overpotential, *ACS Appl. Mater. Interfaces* 14 (2022) 47605–47615, <https://doi.org/10.1021/acscami.2c11911>.
- J. Zeng, D.Z. Wu, X. Wang, J.N. Wu, J.Y. Li, J. Wang, J.B. Zhao, Insights into the Mg storage property and mechanism based on the honeycomb-like structured Na₃V₂(PO₄)₃/C/G in anhydrous electrolyte, *Chem. Eng. J.* 372 (2019) 37–45, <https://doi.org/10.1016/j.cej.2019.04.128>.
- Jin-jie Zhu, W.F.-f.G.U.O.Y.-s.Y.J.N.Y.-n.W.J.-I, Application of ionic liquid PP14TFSI in electrolyte systems for rechargeable Mg batteries, *Journal of Electrochemistry* 20 (2014) 128–133, <https://doi.org/10.13208/j.electrochem.130726>.
- Z. Zhao-Karger, M. Fichtner, Magnesium-sulfur battery: its beginning and recent progress, *MRS Commun* 7 (2017) 770–784, <https://doi.org/10.1557/mrc.2017.101>.
- Z. Zhao-Karger, M. Fichtner, Beyond intercalation chemistry for rechargeable Mg batteries: a short review and perspective, *Front. Chem.* 6 (12) (2019) 656, <https://doi.org/10.3389/fchem.2018.00656>.
- Q.N. Zhao, R.H. Wang, Y.X. Zhang, G.S. Huang, B. Jiang, C.H. Xu, F.S. Pan, The design of Co₃S₄@MXene heterostructure as sulfur host to promote the electrochemical kinetics for reversible magnesium-sulfur batteries, *J. Magnesium Alloys* 9 (2021) 78–89, <https://doi.org/10.1016/j.jma.2020.12.001>.
- L. Kong, C. Yan, J.Q. Huang, M.Q. Zhao, M.M. Titirici, R. Xiang, Q. Zhang, A review of advanced energy materials for magnesium-sulfur batteries, *Energy Environ. Mater.* 1 (2018) 100–112, <https://doi.org/10.1002/eem2.12012>.
- H.S. Kim, T.S. Arthur, G.D. Allred, J. Zajicek, J.G. Newman, A.E. Rodnyansky, A. G. Oliver, W.C. Boggess, J. Muldoon, Structure and compatibility of a magnesium electrolyte with a sulphur cathode, *Nat. Commun.* 2 (6) (2011) 427, <https://doi.org/10.1038/ncomms1435>.
- Y. Xu, Y.F. Ye, S.Y. Zhao, J. Feng, J. Li, H. Chen, A.K. Yang, F.F. Shi, L.J. Jia, Y. Wu, et al., In situ X-ray absorption spectroscopic investigation of the capacity degradation mechanism in Mg/S batteries, *Nano Lett.* 19 (2019) 2928–2934, <https://doi.org/10.1021/acs.nanolett.8b05208>.
- A. Robba, A. Vizintin, J. Bitenc, G. Mali, I. Arcon, M. Kavcic, M. Zitnik, K. Bucar, G. Aquilanti, C. Martineau-Corcoc, et al., Mechanistic study of magnesium-sulfur batteries, *Chem. Mater.* 29 (2017) 9555–9564, <https://doi.org/10.1021/acs.chemmater.7b03956>.
- B.P. Vinayan, H. Euchner, Z. Zhao-Karger, M.A. Cambaz, Z.Y. Li, T. Diemant, R. J. Behm, A. Gross, M. Fichtner, Insights into the electrochemical processes of rechargeable magnesium-sulfur batteries with a new cathode design, *J. Mater. Chem. A* 7 (2019) 25490–25502, <https://doi.org/10.1039/c9ta09155f>.
- W.J. Du, Z.X. Hao, F. Iacoviello, L. Sheng, S.L. Guan, Z.Y. Zhang, D.J.L. Brett, F. R. Wang, P.R. Shearing, A multiscale X-ray tomography study of the cycled-induced degradation in magnesium-sulfur batteries, *Small Methods* 5 (13) (2021) 2001193, <https://doi.org/10.1002/smdt.202001193>.
- R.P. Zhang, C. Cui, R. Xiao, R.A. Li, T.S. Mu, H. Huo, Y.L. Ma, G.P. Yin, P.J. Zuo, Interface regulation of Mg anode and redox couple conversion in cathode by copper for high-performance Mg-S battery, *Chem. Eng. J.* 451 (9) (2023) 138663, <https://doi.org/10.1016/j.cej.2022.138663>.
- M.D. Qian, F.A.L. Laskowski, S.D. Ware, K.A. See, Effect of polysulfide speciation on Mg anode passivation in Mg-S batteries, *ACS Appl. Mater. Interfaces* 15 (2023) 9193–9202, <https://doi.org/10.1021/acscami.2c19488>.
- S.P. Chen, Y.R. Wang, Y.K. Sun, D. Zhang, S.X. Zhang, Y.Z. Zhao, J.L. Wang, J. Yang, Y. Nuli, Research status and prospect of separators for magnesium-sulfur batteries, *J. Energy Chem.* 87 (2023) 225–246, <https://doi.org/10.1016/j.jechem.2023.08.020>.
- T. Gao, X. Ji, S. Hou, X.L. Fan, X.G. Li, C.Y. Yang, F.D. Han, F. Wang, J.J. Jiang, K. Xu, C.S. Wang, Thermodynamics and kinetics of sulfur cathode during discharge in MgTFSI₂-DME electrolyte, *Adv. Mater.* 30 (8) (2018) 1704313, <https://doi.org/10.1002/adma.201704313>.
- Z.Y. Li, A. Welle, S. Vincent, L.P. Wang, S. Fuchs, S. Riedel, A. Roy, D. Bosubabu, J. M. García-Lastra, M. Fichtner, Z. Zhao-Karger, Addressing the sluggish kinetics of sulfur redox for high-energy Mg-S batteries, *Adv. Energy Mater.* 13 (2023) 2302905, <https://doi.org/10.1002/aenm.202302905>.
- X.W. Yu, A. Manthiram, Performance enhancement and mechanistic studies of magnesium-sulfur cells with an advanced cathode structure, *ACS Energy Lett.* 1 (2016) 431–437, <https://doi.org/10.1021/acsenergylett.6b00213>.
- D. Bosubabu, Z.Y. Li, Z. Meng, L.P. Wang, M. Fichtner, Z. Zhao-Karger, Mitigating self-discharge and improving the performance of Mg-S battery in Mg [B(hip)4]2 electrolyte with a protective interlayer, *J. Mater. Chem. A* 9 (2021) 25150–25159, <https://doi.org/10.1039/d1ta06114c>.
- Y. Yang, W. Fu, D. Zhang, W. Ren, S. Zhang, Y. Yan, Y. Zhang, S.-J. Lee, J.-S. Lee, Z.-F. Ma, et al., Toward high-performance Mg-S batteries via a copper phosphide modified separator, *ACS Nano* 17 (2023) 1255–1267, <https://doi.org/10.1021/acsnano.2c09302>.
- L.P. Wang, P. Jankowski, C. Njel, W. Bauer, Z.Y. Li, Z. Meng, B. Dasari, T. Vegge, J. M.G. Lastra, Z. Zhao-Karger, M. Fichtner, Dual role of Mo₆S₈ in polysulfide conversion and shuttle for Mg-S batteries, *Adv. Sci.* 9 (9) (2022) 2104605, <https://doi.org/10.1002/advs.202104605>.
- Y.C. Ji, X. Liu-Théato, Y.L. Xiu, S. Indris, C. Njel, J. Maibach, H. Ehrenberg, M. Fichtner, Z. Zhao-Karger, Polyoxometalate modified separator for performance enhancement of magnesium-sulfur batteries, *Adv. Funct. Mater.* 31 (7) (2021) 2100868, <https://doi.org/10.1002/adfm.202100868>.
- T. Mandai, Critical issues of fluorinated alkylborate-based electrolytes in magnesium battery applications, *ACS Appl. Mater. Interfaces* 12 (2020) 39135–39144, <https://doi.org/10.1021/acscami.0c09948>.
- H.O. Ford, E.S. Doyle, P. He, W.C. Boggess, A.G. Oliver, T.P. Wu, G.E. Sterbinsky, J. L. Schaefer, Self-discharge of magnesium-sulfur batteries leads to active material loss and poor shelf life, *Energy Environ. Sci.* 14 (2021) 890–899, <https://doi.org/10.1039/d0ee01578d>.
- M.J. Frisch, G.W. Trucks, H.B. Schlegel, G.E. Scuseria, M.A. Robb, J.R. Cheeseman, G. Scalmani, V. Barone, B. Mennucci, G.A. Petersson, et al., *Gaussian 09, Revision E.01*, Gaussian, Inc., Wallingford CT, 2013.
- P.J. Stephens, F.J. Devlin, C.F. Chabalowski, M.J. Frisch, AB-INITIO calculation of vibrational absorption and circular-dichroism spectra using density-functional force-fields, *J. Phys. Chem.* 98 (1994) 11623–11627, <https://doi.org/10.1021/j100096a001>.
- S. Grimme, J. Antony, S. Ehrlich, H. Krieg, A consistent and accurate ab initio parametrization of density functional dispersion correction (DFT-D) for the 94 elements H-Pu, *J. Chem. Phys.* 132 (19) (2010) 154104, <https://doi.org/10.1063/1.3382344>.
- F. Weigend, R. Ahlrichs, Balanced basis sets of split valence, triple zeta valence and quadruple zeta valence quality for H to Rn: design and assessment of accuracy, *Phys. Chem. Chem. Phys.* 7 (2005) 3297–3305, <https://doi.org/10.1039/b508541a>.
- T. Lu, F.W. Chen, Multiwfn: a multifunctional wavefunction analyzer, *J. Comput. Chem.* 33 (2012) 580–592, <https://doi.org/10.1002/jcc.22885>.
- R. Richter, J. Häcker, Z.R. Zhao-Karger, T. Danner, N. Wagner, M. Fichtner, K. A. Friedrich, A. Latz, Insights into self-discharge of lithium- and magnesium-sulfur batteries, *ACS Appl. Energy Mater.* 3 (2020) 8457–8474, <https://doi.org/10.1021/acsaem.0c01114>.
- J. Häcker, D.H. Nguyen, T. Rommel, Z. Zhao-Karger, N. Wagner, K.A. Friedrich, Operando UV/vis spectroscopy providing insights into the sulfur and polysulfide dissolution in magnesium-sulfur batteries, *ACS Energy Lett.* 7 (2022) 1–9, <https://doi.org/10.1021/acsenergylett.1c02152>.
- J. Häcker, C. Danner, B. Sievert, I. Biswas, Z. Zhao-Karger, N. Wagner, K. A. Friedrich, Investigation of magnesium-sulfur batteries using electrochemical impedance spectroscopy, *Electrochim. Acta* 338 (12) (2020) 135787, <https://doi.org/10.1016/j.electacta.2020.135787>.
- H.J. Tian, T. Gao, X.G. Li, X.W. Wang, C. Luo, X.L. Fan, C.Y. Yang, L.M. Suo, Z. H. Ma, W.Q. Han, C.S. Wang, High power rechargeable magnesium/iodine battery

- chemistry, *Nat. Commun.* 8 (8) (2017) 14083, <https://doi.org/10.1038/ncomms14083>.
- [41] D.Z. Wu, Y.C. Zhuang, F. Wang, Y. Yang, J. Zeng, J.B. Zhao, High-rate performance magnesium batteries achieved by direct growth of honeycomb-like V₂O₅ electrodes with rich oxygen vacancies, *Nano Res.* 16 (2023) 4880–4887, <https://doi.org/10.1007/s12274-021-3679-2>.
- [42] Y.S. Liu, X. Liu, S.M. Xu, Y.L. Bai, C. Ma, W.L. Bai, X.Y. Wu, X. Wei, K.X. Wang, J. S. Chen, 3D ordered macroporous MoO₂ attached on carbonized cloth for high performance free-standing binder-free lithium-sulfur electrodes, *J. Mater. Chem. A* 7 (2019) 24524–24531, <https://doi.org/10.1039/c9ta08498c>.
- [43] J.H. Hou, C.B. Cao, F. Idrees, X.L. Ma, Hierarchical porous nitrogen-doped carbon nanosheets derived from silk for ultrahigh-capacity battery anodes and supercapacitors, *ACS Nano* 9 (2015) 2556–2564, <https://doi.org/10.1021/nm506394r>.
- [44] P. He, H.O. Ford, S. Gonzalez, S. Rodriguez, A.G. Oliver, J.L. Schaefer, Stability and disproportionation of magnesium polysulfides and the effects on the Mg-polysulfide flow battery, *J. Electrochem. Soc.* 168 (10) (2021) 110516, <https://doi.org/10.1149/1945-7111/ac33e2>.
- [45] M. Lee, M. Jeong, Y.S. Nam, J. Moon, M. Lee, H.D. Lim, D. Byun, T. Yim, S.H. Oh, Nitrogen-doped graphitic mesoporous carbon materials as effective sulfur imbibition hosts for magnesium-sulfur batteries, *J. Power Sources* 535 (9) (2022) 231471, <https://doi.org/10.1016/j.jpowsour.2022.231471>.
- [46] X. Wu, Y. Du, P.X. Wang, L.S. Fan, J.H. Cheng, M.X. Wang, Y. Qiu, B. Guan, H. X. Wu, N.Q. Zhang, K.N. Sun, Kinetics enhancement of lithium-sulfur batteries by interlinked hollow MoO₂ sphere/nitrogen-doped graphene composite, *J. Mater. Chem. A* 5 (2017) 25187–25192, <https://doi.org/10.1039/c7ta08859k>.
- [47] D.-Q. Cai, Y.-T. Gao, X.-Y. Wang, J.-L. Yang, S.-X. Zhao, Built-in electric field on the mott-Schottky heterointerface-enabled fast kinetics lithium-sulfur batteries, *ACS Appl. Mater. Interfaces* 14 (2022) 38651–38659, <https://doi.org/10.1021/acsami.2c06676>.
- [48] W.W. Yang, Y. Wei, Q. Chen, S.J. Qin, J.H. Zuo, S.D. Tan, P.B. Zhai, S.Q. Cui, H. W. Wang, C.Q. Jin, et al., A MoO₃/MoO₂-CP self-supporting heterostructure for modification of lithium-sulfur batteries, *J. Mater. Chem. A* 8 (2020) 15816–15821, <https://doi.org/10.1039/d0ta01664k>.
- [49] R.K. Bhardwaj, R. Gomes, A.J. Bhattacharyya, Probing the polysulfide confinement in two different sulfur hosts for a Mg|S battery employing operando Raman and ex-situ UV- visible spectroscopy, *J. Phys. Chem. Lett.* 13 (2022) 1159–1164, <https://doi.org/10.1021/acs.jpclett.1c03958>.
- [50] J. Guo, H.L. Jiang, M. Yu, X.C. Li, Y. Dai, W.J. Zheng, X.B. Jiang, G.H. He, Sandwich-Structured flexible interlayer with Co₃O₄ nanoboxes strung along carbon nanofibers on both sides for fast Li plus transport and high redox activity in High-Rate Li-S batteries, *Chem. Eng. J.* 449 (12) (2022) 137777, <https://doi.org/10.1016/j.cej.2022.137777>.
- [51] H.X. Li, S. Ma, H.Q. Cai, H.H. Zhou, Z.Y. Huang, Z.H. Hou, J.J. Wu, W.J. Yang, H. B. Yi, C.P. Fu, Y.F. Kuang, Ultra-thin Fe₃C nanosheets promote the adsorption and conversion of polysulfides in lithium-sulfur batteries, *Energy Storage Mater.* 18 (2019) 338–348, <https://doi.org/10.1016/j.ensm.2018.08.016>.
- [52] A. Robba, M. Meznar, A. Vizintin, J. Bitenc, J. Bobnar, I. Arcon, A. Randon-Vitanova, R. Dominko, Role of Cu current collector on electrochemical mechanism of Mg-S battery, *J. Power Sources* 450 (7) (2020) 227672, <https://doi.org/10.1016/j.jpowsour.2019.227672>.
- [53] X. Liu, Y. Li, X. Xu, L. Zhou, L.Q. Mai, Rechargeable metal (Li, Na, Mg, Al)-sulfur batteries: materials and advances, *J. Energy Chem.* 61 (2021) 104–134, <https://doi.org/10.1016/j.jechem.2021.02.0282095-4956/>.
- [54] Y. Lu, C. Wang, Q. Liu, X.Y. Li, X.Y. Zhao, Z.P. Guo, Progress and perspective on rechargeable magnesium-sulfur batteries, *Small Methods* 5 (24) (2021) 2001303, <https://doi.org/10.1002/smt.202001303>.
- [55] U. Chadha, P. Bhardwaj, S. Padmanaban, D. Kabra, G. Pareek, S. Naik, M. Singh, M. Banavoth, P. Sonar, S. Singh, et al., Review-carbon electrodes in magnesium sulphur batteries: performance Comparison of electrodes and future directions, *J. Electrochem. Soc.* 168 (27) (2021) 120555, <https://doi.org/10.1149/1945-7111/ac4104>.
- [56] D.T. Nguyen, R. Horia, A.Y.S. Eng, S.W. Song, Z.W. Seh, Material design strategies to improve the performance of rechargeable magnesium-sulfur batteries, *Mater. Horiz.* 8 (2021) 830–853, <https://doi.org/10.1039/d0mh01403f>.
- [57] Y.Y. Yao, Y. Zhan, X.Y. Sun, Z. Li, H. Xu, R.M. Laine, J.X. Zou, Advances in cathodes for high-performance magnesium-sulfur batteries: a critical review, *Batteries-Basel* 9 (19) (2023) 203, <https://doi.org/10.3390/batteries9040203>.
- [58] Z. Zhao-Karger, X.Y. Zhao, D. Wang, T. Diemant, R.J. Behm, M. Fichtner, Performance improvement of magnesium sulfur batteries with modified non-nucleophilic electrolytes, *Adv. Energy Mater.* 5 (9) (2015) 1401155, <https://doi.org/10.1002/aenm.201401155>.